Earth, Planets and Space

FULL PAPER Open Access

Lightning evolution and VLF perturbations associated with category 5 TC Yasa in the South Pacific Region

Paolo A. A. L. Redoblado, Sarwan Kumar, Abhikesh Kumar* and Sushil Kumar

Abstract

In this paper, we present the D-region ionospheric response during the lifespan (10–19 December 2020) of a severe category 5 tropical cyclone (TC) Yasa in the South Pacific by using the very low frequency (VLF, 3–30 kHz) signals from NPM, NLK, and JJI transmitters recorded at Suva, Fiji. Results indicate enhanced lightning and convective activity in all three regions (eyewall, inner rainbands, and outer rainbands) during the TC Yasa that are also linked to the wave-sensitive zones of these transmitter–receiver great circle paths. Of the three regions, the outer rainbands showed the maximum lightning occurrence; hence convective activity. Prominent eyewall lightning was observed just before the TC started to weaken following its peak intensity. Analysis of VLF signals amplitude showed both negative and positive perturbations (amplitudes exceeding $\pm 3\sigma$ mark) lasting for more than 2 h with maximum change in the daytime and nighttime signal amplitudes of -4.9 dB (NPM) and -19.8 dB (NLK), respectively. The signal perturbations were wave-like, exhibiting periods of oscillations between ~ 2.2 and 5.5 h as revealed by the Morlet wavelet analysis. Additionally, the LWPC modeling of the signal perturbations indicated a 10 km increase in the daytime D-region reference height, H', and a 12 km decrease in the nighttime D-region H' during TC Yasa. The D-region density gradients (sharpness), β, showed small perturbations of 0.01–0.14 km^{-1} from its normal values. We suggest that the observed changes to the D-region parameters are due to the enhanced convection during TC Yasa which excites atmospheric gravity waves producing traveling ionospheric disturbances to the D-region.

Keywords: VLF perturbations, Lightning, D-region, Tropical cyclones

*Correspondence: abhikesh.kumar@usp.ac.fj
School of Information Technology, Engineering, Mathematics and Physics (STEMP), The University of the South Pacific, Suva, Fiji

Graphical Abstract

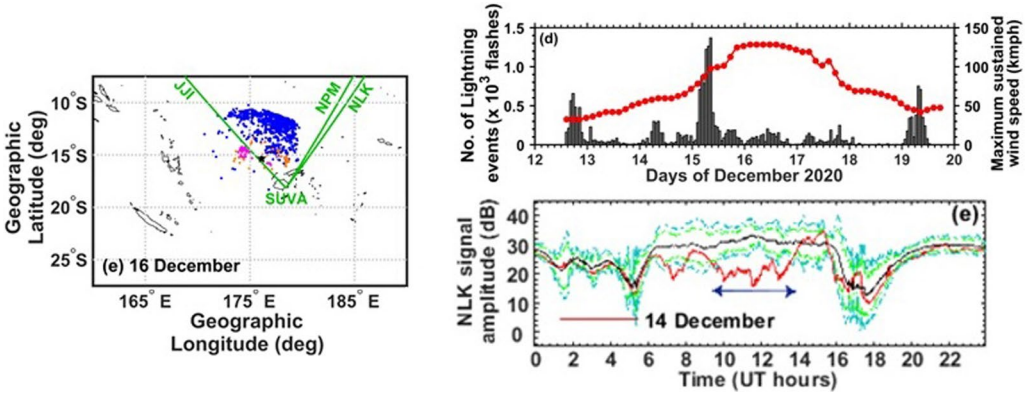

Introduction

Tropical cyclones (TCs) are one of the leading natural disasters in the South Pacific Region. These immense and powerful convective storms have the potential to claim the lives of people, cause damages to physical structures and agriculture, and disrupt the overall socio-economic livelihood of the small and vulnerable Pacific Island Countries (PICs). A TC is a rapidly rotating storm system characterized by a low-pressure center, strong winds, and a spiral organization of thunderstorms that produce heavy rain. TCs can have total lifetimes from a few days to 2–3 weeks at most and generally spend most of their lifetime over the oceans.

Very low frequency (VLF, 3–30 kHz) navigational transmitters situated in different regions of the world radiate electromagnetic signals which propagate through the earth-ionosphere waveguide (EIWG) by multiple reflections with a low attenuation rate of 2–3 dB/Mm (Wait 1962). The VLF signals from these transmitters have been widely used in several investigations relating to the D-region ionospheric effects associated with phenomena occurring from above the ionosphere, such as geomagnetic storms (Kerrache et al. 2021), solar flares (Selvakumaran et al. 2015), solar eclipses (Venkatesham et al. 2019), gamma ray bursts (Nina et al. 2015), and soft gamma ray repeaters (Mondal et al. 2012), as well as those occurring from below it, such as earthquakes (Hayakawa 2015; Kumar et al. 2013), lightning discharges (Rodger 2003; Kumar et al. 2008), and TCs (Rozhnoi et al. 2014). In particular, the use of VLF signals to investigate the D-region response to TCs is mainly based on monitoring sudden ionospheric disturbances during TCs which are observed in terms of signal perturbations over short time scales of 1–100 s or a few minutes. These VLF signal investigations can be broadly generalized as either determining the intensity of lightning flashes as a precursor to cyclone intensification/weakening (e.g., Price et al. 2007) or analyzing the lightning activity surrounding TCs (e.g., Thomas et al. 2010). Apart from lightning, atmospheric gravity waves (AGWs) and acoustic GWs excited by TCs have also been reported as an alternate process, whereby TCs influence variations in the D-region for which the VLF signals are sensitive to (Kumar et al. 2017; NaitAmor et al. 2018).

There have been studies relating to the possible D-region ionospheric response to the action of intense TCs beginning with the work by Bauer (1958). Isaev et al. (2002) and Thomas et al. (2010) suggested that the possible coupling between the lower ionosphere and TCs may be due to electrical and electromagnetic effects, particularly at low latitudes (temperate latitudes). Further investigations towards TCs effects in the lower ionosphere done by Rozhnoi et al. (2014) have shown meteorological relationships after analyzing the VLF signals of navigational transmitters JJI, JJY, NWC, and NPM recorded in three far eastern stations in Russia. They looked at eight TCs of varying intensities and found negative nighttime anomalies in the signal amplitude for six events that were most probably caused by TC activity which significantly correlated with the variations of atmospheric pressure, temperature, humidity, and wind velocity. Kumar et al. (2017) studied the TC Evan when it was within the proximity of the transmitter–receiver links (NPM, NLK, NAA, and JJI) to Suva between 9 to 16 December 2012 and found signal amplitude perturbations associated with the decrease and increase in the nighttime and daytime D-region reference height, H'. They also highlighted a very clear transition of wave-like signature events from quiet to TC disturbed days exhibiting characteristics similar to GWs. Similarly, based on investigations towards

ionospheric disturbances during large meteorological systems (hurricanes and TCs), NaitAmor et al. (2018) observed TC anomalies in VLF signal amplitudes during both day and night and highlighted that the signal anomalies were detected even at the early stages of the TC (depression). They inferred that the signal anomalies may result from traveling ionospheric disturbances (TIDs) generated by TC/hurricane associated AGWs. In a more recent study, Das et al. (2021) determined D-region ionospheric disturbances due to TC Fani over the Indian Ocean based on three VLF transmitter signals (JJI, NWC, and VTX) received at two low-latitude stations and found strong amplitude perturbations beyond 3σ mark which consistently correlated with the wind speed and central pressure of the TC. Although there has been great progress towards characterizing the coupling between TCs and the D-region, little has been done in determining the source origins of these coupling mechanisms, in particular, the convective sources of TC-induced AGWs which is the focus of this study.

In this paper, we present the lightning evolution pattern associated with TC Yasa which occurred during the 2020 cyclone season of the Southwest Pacific. We have used the World Wide Lightning Location Network (WWLLN) data to plot the lightning flash density for this cyclone from 12 to 19 December 2020. The wind speed measurements from National Oceanic and Atmospheric Administration (NOAA) have also been used to estimate the storm intensity of the TC. The VLF anomalies during TC Yasa have been modeled using the Long Wavelength Propagation Capability (LWPC) code V2.1 to determine the associated ionospheric D-region perturbations. We attempt to determine the possible meteorological origins of AGWs during TC Yasa by analyzing the lightning events during the active period of the storm.

Brief description of TC Yasa

According to the National Disaster Management Office and Fiji Red Cross Society, three tropical depressions (TDs) formed from 10 to 13 December 2020, namely, TD01F, TD02F, and TD03F, with TC Yasa developing from TD02F. From the cyclone wind measurements by NOAA, TD02F developed into a category 1 strength on 14 December at about 6:00 UT. On 15 December, TC Yasa intensified to a category 2 TC (~0:00 UT), then developed into category 3 TC around 6:00 UT. TC Yasa then slowly intensified into a category 4 TC at about 15:00 UT after creating a loop west of Port Vila, Vanuatu (17.73° S, 168.33° E). Later, TC Yasa turned to the southeast direction and reached its peak intensity of category 5 TC around 21:00 UT. TC Yasa maintained its peak intensity for about 18 h until it was classified back to category 4 TC on 16 December at 18:00 UT. TC Yasa then continued southeast and crossed over the second mainland (Vanua Levu) of the Fiji Islands. On 17 December, TC Yasa moved away from Vanua Levu and faded into category 3 TC at 15:00 UT. The storm intensity dropped to category 2 at 18:00 UT and later to category 1 at 21:00 UT. It weakened back to a TD on 18 December at about 21:00 UT and continued in its southern path. The storm path and intensity of TC Yasa are shown as an inset image in Fig. 1.

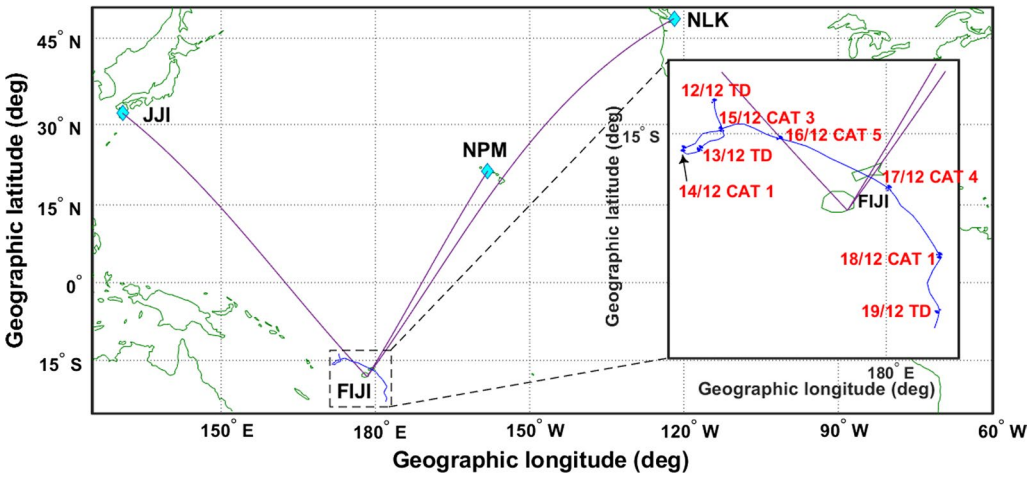

Fig. 1 The relative location of the three VLF transmitters (JJI, NPM, and NLK) in cyan diamond and a receiver station (Fiji) together with their transmitter–receiver great circle path (purple). The zoom portion shows the TC Yasa path (blue line) with different strengths and dates marked in red which were recorded at 12 UT on each day starting from 12 to 19 December 2020

Data and analysis

The lightning data were obtained from the WWLLN database which is a global lightning location detection network. The WWLLN provides nearly real-time lightning locations in terms of geographical location (latitude and longitude) and occurrence date and time (dd/mm/yyyy hh:mm:ss UT) of lightning strokes detected by this network. For a lightning stroke to be accurately detected with error analysis, the VLF radiation from a lightning discharge must be detected by a minimum of five of the network's over 80 receivers around the world (Holzworth et al. 2019). The WWLLN data processed using the upgraded (version 2) algorithm, which gives the network a location accuracy of less than 10 km and 10 μs (Rodger et al. 2009) for each lightning stroke, have been used. With the version 2 algorithm and the increase in the number of WWLLN stations over the years as of 2010, it is estimated that the network's detection efficiency has increased to 11% for all lightning strokes and > 30% for strokes with peak currents > ± 35 kA (Abarca et al. 2010; Bürgesser 2017; Hutchins et al. 2012). The lightning flash density for each day (24 h) for the period 12 to 19 December 2020 were plotted using Matlab codes to determine the daily spatial distribution and also used to study temporal evolution during the storm period. To help locate and identify the possible convective source regions within the storm, the lightning distributions were determined for three radial regions centered on the eye of the TC (Zhang et al. 2012); the eyewall (radius, $r = 60$ km), inner rainband ($r = 60$ to 80 km) and outer rainband ($r = 180$ to 500 km). In addition, the hourly counts of lightning flashes for the three radial regions were also determined during the lifetime of TC Yasa. This was done by first binning the lightning events in a ¼° × ¼° grid cells centered on the TC eye. The number of lightning events occurring inside each region within a 1-h time window was then counted and recorded.

TC Yasa moved towards Fiji and intercepted the VLF paths from transmitters in Japan (JJI), Hawaii (NPM), and the USA (NLK) to Suva station. Over 16 days (from 10 to 25 December 2020) of VLF data from the mid-latitude (JJI & NLK) and low-latitude (NPM) transmitters and recorded at the VLF receiver located at Suva, Fiji (18.14° S, 178.44° E) were used to analyze the TC Yasa's effect on the lower ionosphere (D-region). The relative location of the three VLF transmitters (JJI, NPM, and NLK), the receiving station, their transmitter–receiver great circle paths (TRGCPs), and the TC Yasa track are shown in Fig. 1. The receiver station consists of the magnetic GPS antenna with a clear view of the sky and an electric field antenna made up of a 5-m-long vertical copper wire of 1 mm diameter enclosed in a PVC pipe. The bottom end of the copper wire is attached to the E-field pre-amplifier, which is connected to the GPSNanoSync (GNS) unit. The GNS unit is attached to a computer installed with a software based amplitude and phase logger termed as SoftPAL that can record narrowband data of 10–100 ms resolution at seven frequencies at the same time (Dowden and Adams 2008). Here, we present the amplitude perturbation using 1 min averaged data from the recording at 100 ms resolution. To determine the signal perturbations, we first established the baseline amplitude values of the VLF signals by averaging the signal amplitudes during five international quiet days (Q-days) in December 2020. The geomagnetically quiet and disturbed days were on 1, 2, 3, 4, 7, 15, 16, 17, 18, 31, and 21, 22, 23, 24, 30, respectively, in December. Due to the four quiet days out of 10 above involved during the TD/TC period, and the limitation of VLF data availability, we have only used the five Q-days average. The five Q-days were obtained from the World Data Centre website http://wdc.kugi.kyoto-u.ac.jp/ which provides information relating to the daily level of geomagnetic activity based on disturbance storm time (D_{st}) and K_p indices. Periods of high geomagnetic activity ($D_{st} < -50$nT) are known to strongly disturb the ionosphere at middle- and low-latitudes (Huang et al. 2005; Qian et al. 2019) and have been observed to significantly perturb VLF signals (e.g., Choudhury et al. 2015). Hence, data from the World Data Centre have been used to recognize and remove such periods in our analysis to minimize the influence of high geomagnetic activity in the VLF signal variability. The period during TD/TC was geomagnetically quiet and perturbations beyond 1σ may also be considered as TC-associated anomalies, but for stronger confidence (99.7%), perturbations beyond ± 3σ (plus and minus, three times the standard deviations) were considered for the analysis. The ± 3σ value is determined by adding and subtracting 3σ (of the Q-days) to the averaged values of Q-days for every minute. If the VLF signal amplitudes exceeded more than three standard deviation (± 3σ) for ≥ 2 h, then these perturbations were considered TC-associated VLF signal anomalies. The difference between the perturbed amplitude A_P during the TC and the baseline amplitude A_B of the signals defined as $\Delta A = A_P - A_B$ is also determined and is referred here as the reduced signal amplitude.

To find the response of the lower ionospheric D-region during TC Yasa, the Long Wave Propagation Capability V2.1 (LWPC) code was used to model the characteristics of detected VLF signal perturbations of the NPM transmitter (Ferguson 1998). The code considers the EIWG to behave as a parallel-plate structure bounded below by an imperfect ground and above by ionospheric D-region plasma. For a given VLF wave propagation path, the code divides the path into segments and sequentially calculates at each segment the wave electric field intensity starting

from the transmitter and ending at the receiver by using the path conductivity and permittivity data embedded in the code. Wait model of the lower ionosphere which parameterizes the region in terms of the sharpness (β in km^{-1}) and reference height (H' in km) (Wait and Spies 1964) has been used. The disturbed segment is determined by projecting the TC eye onto the signal propagation path. It is assumed that the path segment closest to the TC center at the time of signal perturbation would experience the greatest ionospheric disturbance (Das et al. 2021; Pal et al. 2020). This path segment is found by determining the minimum distance between the TC center and each of the segments generated by the LWPC code. The disturbance along the signal path is approximated in this study to extend up to 1000 km on either direction from the disturbed segment similar to the approximations done by Das et al. (2021) and Kumar et al. (2017). The characteristics of the detected VLF signal perturbation in terms of its magnitude in the amplitude and phase are then used to introduce a localized perturbation to the Wait parameters of the disturbed segment. In this analysis, the perturbation to the Wait parameters is assumed to display a Gaussian distribution and the process is iterated until a best-fit is found between the amplitude and phase of the real-time and code-simulated signals. Our use of the LWPC code considers the quality of fit with respect to the magnitude of perturbation to the signal rather than the values between the real-time and simulated signal. This is achieved by determining a unique pair of Wait parameters such that the code-simulated signal falls within a specified range of the magnitudes of the perturbations to the signal amplitude (± 0.5 dB) and phase ($\pm 5°$).

Finally, the signatures of the wave-like structures (WLS) present in the VLF signal amplitudes (NPM, NLK, and JJI) during 10 to 25 December were then estimated using the mother Morlet wavelet technique to determine their association with AGWs (Mallat 1999). Specifically, the spectra were determined only for the complete daytime and nighttime periods of the TRGCPs considering that solar terminator transition periods generate AGWs (Nina and Čadež 2013). The duration used for daytime is, NPM: 20–03 h UT, NLK: 19–00 UT, JJI: 22–06 UT and nighttime is, NPM: 07–16 UT, NLK: 07–16 UT, JJI 09–17 UT. For a given signal $x(t,z)$ with amplitude z and time series t, the wavelet transform $T_x(a,u,z)$ is defined as:

$$T_x(a,u,z) = \frac{1}{\sqrt{a}} \int_{-\infty}^{+\infty} x(t,z)\psi^*\left(\frac{t-u}{a}\right) \mathrm{d}t,$$

where ψ is the mother Morlet wavelet function, a (positive value) is the scale of the analyzing wavelet, and u is the wavelet shift parameter. For further details regarding the wavelet transform, the reader is referred to Mallat (1999) and Addison (2017).

Results

Lightning evolution during TC Yasa

Figure 2 shows the daily spatial and temporal variation of lightning occurrence for three radial regions centered on the TC eye, namely, the eyewall (pink dots), the inner (orange dots) and the outer (blue dots) rainbands of TC Yasa from 12 to 19 December 2020. It can be observed that the majority of the lightning events took place in the outer rainband as seen from 12 to 17 December. The flashes of lightning in the outer rainband populated along the JJI signal path during the early days of TC Yasa from 12 to 15 December and later along the NPM and NLK signal paths on 17 December. Comparatively weaker outer rainband lightning activity can be seen during the weakening phase of TC Yasa from 18 to 19 December. Lightnings in the inner rainband occurred more frequently during the early days of TC Yasa from 12 to 14 December and decreased mainly to the right side of the JJI-Suva path. The inner rainband lightning density decreased as the days passed with a sudden increase at the end of TC Yasa on 19 December. Very few eyewall lightnings were observed throughout the lifetime of the storm. Prominent occurrence of eyewall lightning activity can be seen on 16 and 17 December during which TC Yasa reached peak intensity and slowly weakened with its movement towards the south of Fiji. If we relate the density of lightning locations with the regions of convective activity within TC Yasa, it can be inferred that convective activities were close to or were within the sensitive zones of the three VLF transmitters and that the density of convective activities is mostly in the outer rainband of the TC. The hourly variation of lightning activity within the three radial regions and for the total region as presented in Fig. 3 showed a change in the intensity of the storm varying with maximum sustained wind speeds. The maximum peak in lightning activity for the outer rainband occurred approximately one day before the peak in maximum wind speed (Fig. 3c). For the eyewall and inner rainband, however, the maximum peak in lightning activity occurred after the peak in maximum sustained winds. The peak in lightning activity in the eyewall occurred several hours after the cyclone started weakening (Fig. 3b), whereas the peak in lightning activity in the inner rainband occurred approximately 2 days after (Fig. 3c) when the TC was in its weakening phase.

VLF signal analysis during TC Yasa: December 2020

NPM signal amplitude analysis

The signal from the NPM transmitter (21.4 kHz) propagates across the geomagnetic equator over the ocean

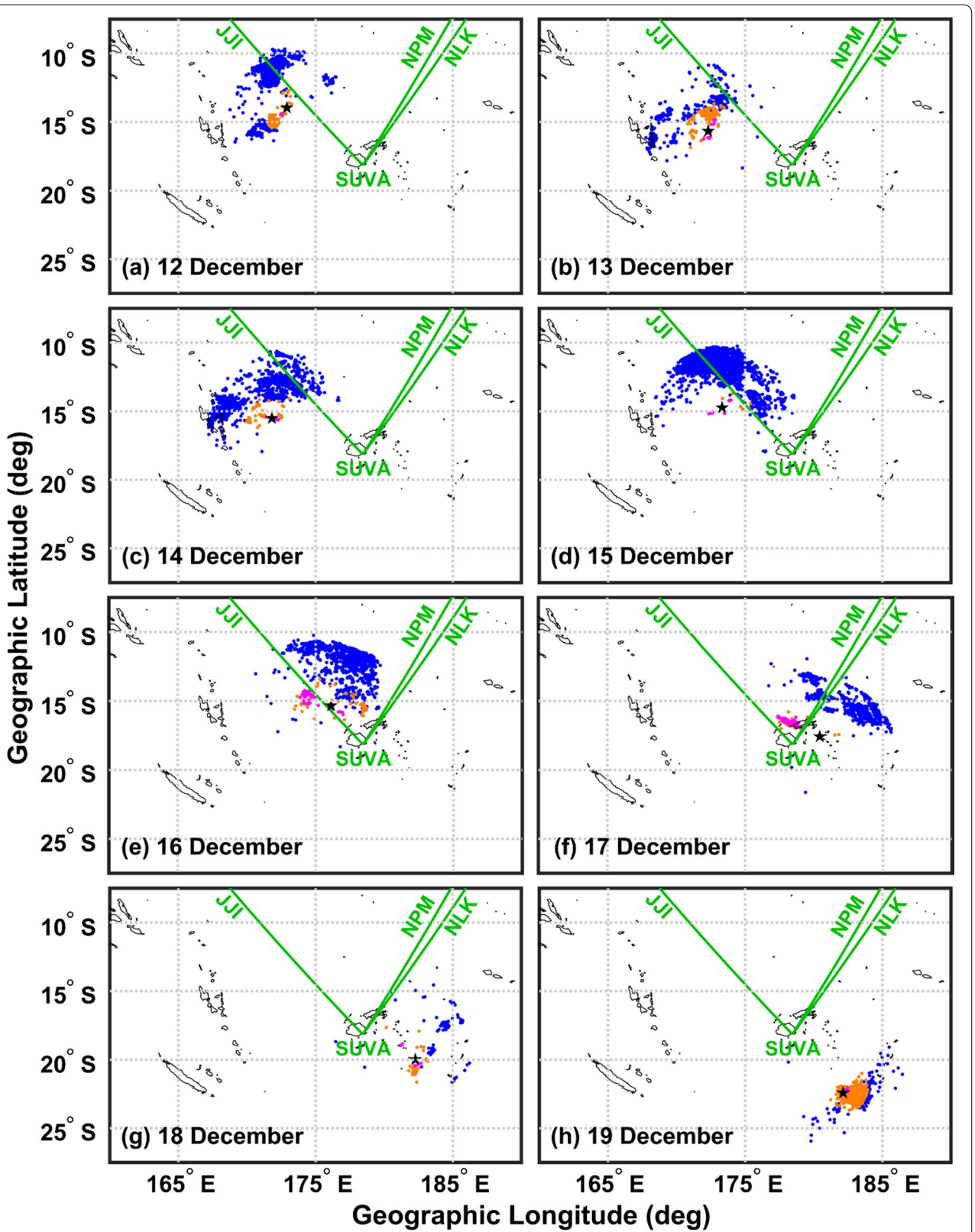

Fig. 2 **a**–**h** Spatial and temporal variation of lightning during TC Yasa from 12 to 19 December 2020. Lightning activity is quantified in three radial regions centered on the eye of the TC; the eye wall (magenta), inner rainband (orange) and outer rainband (blue). The location of the TC eye at 15:00 UT on each day is indicated by the black star. The JJI, NPM and NLK signal paths to Suva receiver in green are also shown

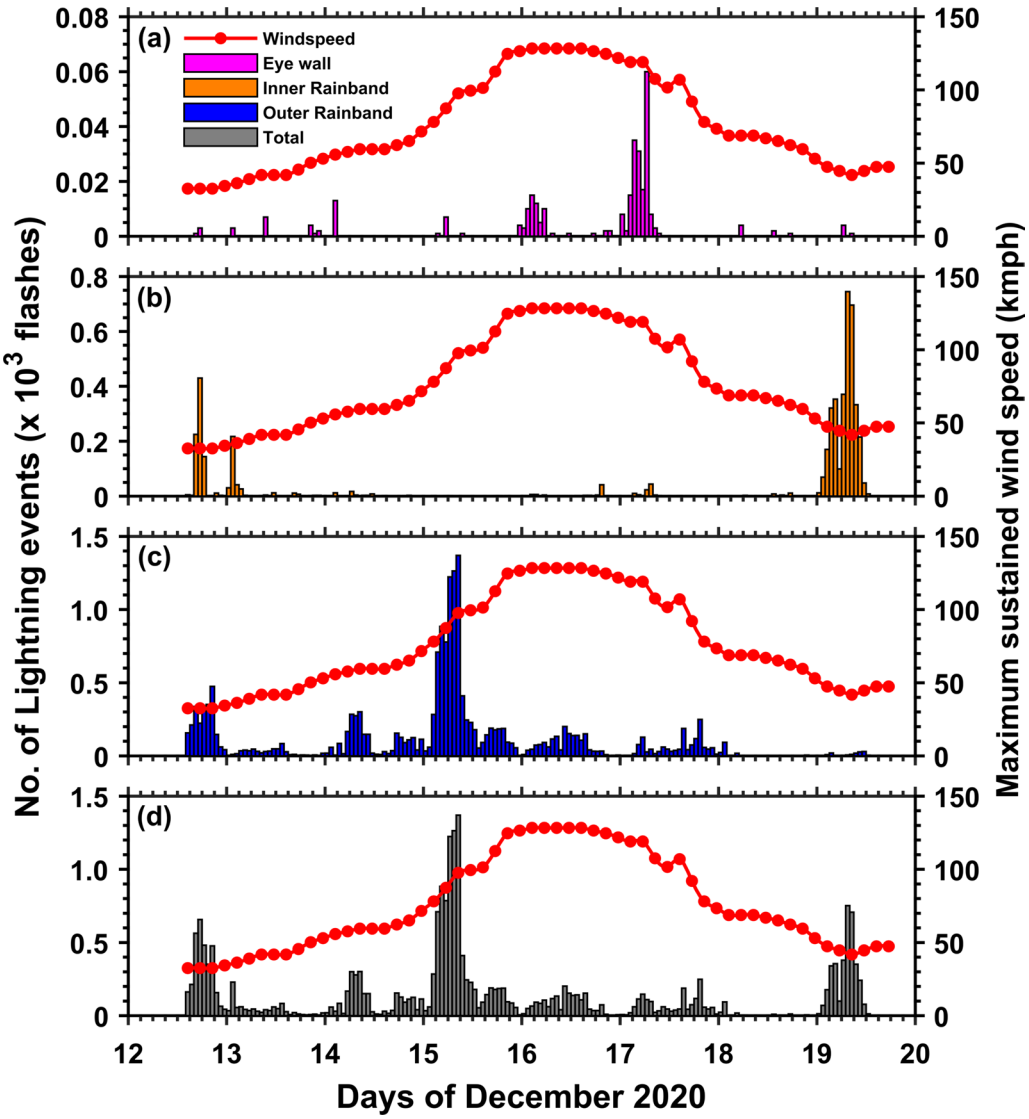

Fig. 3 Hourly intensity variation of TC Yasa based on lightning activity and maximum sustained wind speeds from 12 (15:00 UT) to 19 (16:00 UT) December 2020. Lightning activity is quantified in three radial regions centered on the eye of the TC: **a** the eyewall, **b** inner rainband and **c** outer rainband. The total lightning activity in the three regions of the TC is shown in **d**

mainly in north to south direction and fairly less in east to west direction to Suva, with a complete path length of 5.07 Mm. Figure 4 shows the diurnal plots of the NPM signal amplitude (panels a-p) during the main phase of TC Yasa (12–19 December) along with 2 days before the cyclone (10–11 December) and 6 days post-cyclone (20–25 December). The diurnal plot of the NPM signal phase as recorded by SoftPAL at our station on 11 December is also shown in panel b of Fig. 4 where the characteristic amplitude fadings and step changes in phase during terminator times can be seen (Crombie 1964). The large values of the phase (few orders of ten) as seen from the plot are the ones correctly generated by SoftPAL and its not necessary to divide by 10. The phase recorded at our station becomes unstable and builds up to large values over time. However, this has not affected our analysis and modeling results since we only required the change in phase ($\Delta\phi$) during the perturbations. The time is in UT and the local time in Fiji is LT = UT + 12:00 h. In each panel, the black line represents the mean signal amplitude on five international geomagnetic Q-days for the observed cyclone month and the red line is the real-time signal amplitude for the days indicated. The green and cyan dashed lines indicate the $\pm 2\sigma$ and $\pm 3\sigma$ Q-days

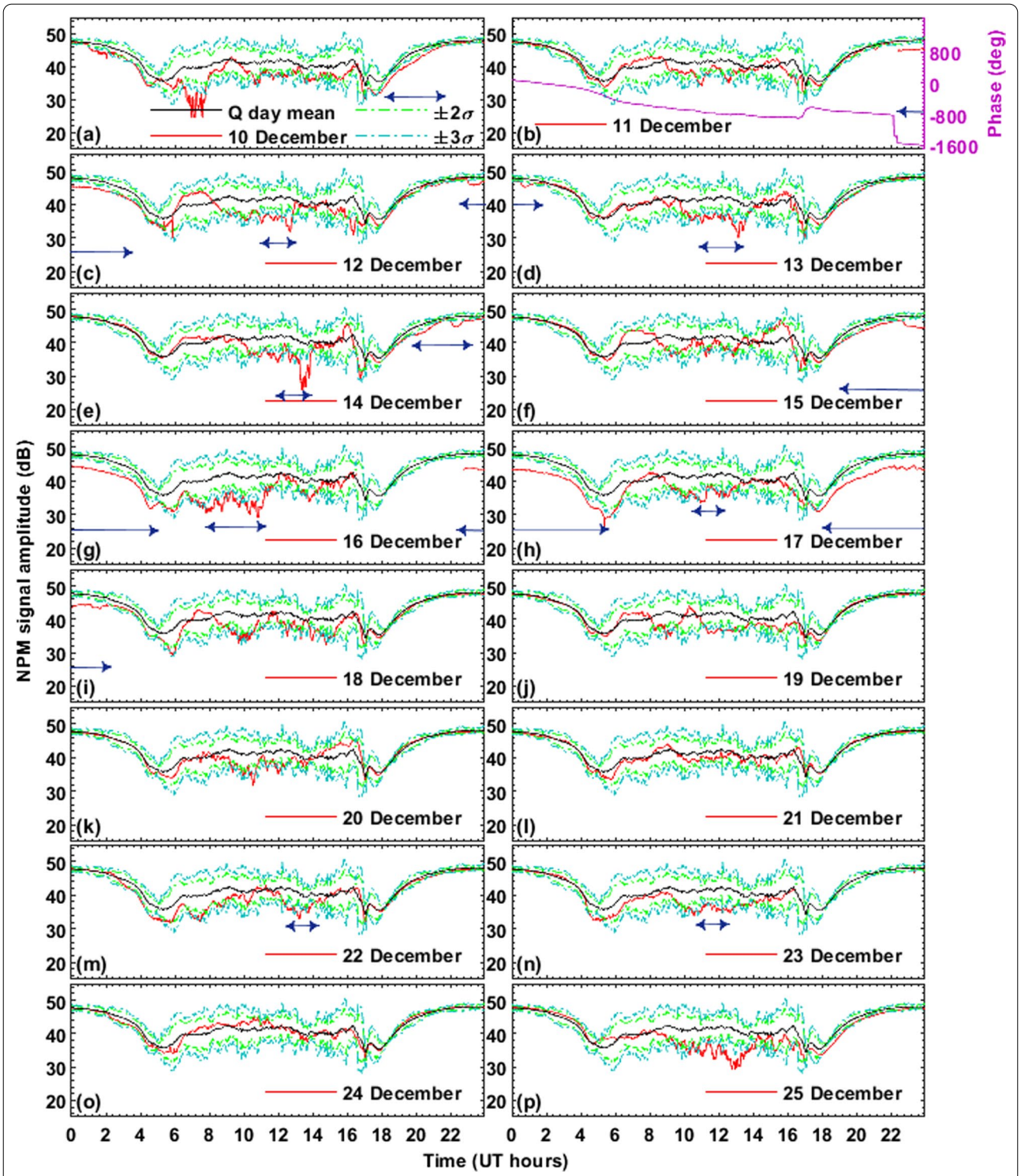

Fig. 4 **a**–**p** NPM signal amplitude (red) during 10 to 25 December 2020 which includes TC Yasa days. The mean signal amplitude for five quiet days (black) along with the ± 2σ (green) and ± 3σ (cyan) are shown. The NPM signal phase on 11 December is shown in purple. Signal amplitude perturbations are marked with blue horizontal arrows

signal amplitudes, respectively, which define the 95% and 99.7% confidence levels of signal variability, respectively. The threshold for the VLF anomalies due to the storm phase is marked with a blue arrow where perturbed amplitude exceeds $\pm 3\sigma$ level for more than 2 h. The periods of transmitter being off-air are removed from the plots. From the NPM amplitude, anomalies are identified when signal amplitude went below the -3σ line during the daytime and nighttime.

Several clear anomalies for NPM signal amplitude below the -3σ line were observed during the TC. The first anomaly occurred when TC Yasa was a TD on 10 December. The daytime signal amplitude began decreasing -3σ line at 17:46 UT and approached -3σ line at 21:37 UT, where the maximum anomaly was observed at 19:30 UT ($\Delta A = -3.2$ dB). On 11–12 December, the amplitude decreased below the -3σ line for the period 22:24–2:22 UT, where the maximum signal anomaly was observed at 0:05 UT with $\Delta A = -2.6$ dB. On 12 December, the nighttime signal amplitude declined -3σ line for ~ 2 h, where the maximum signal anomaly was observed at 12:41 UT with $\Delta A = -10.0$ dB. During the daytime on 12–13 December, the maximum amplitude anomaly beyond -3σ line was observed at 23:24 UT ($\Delta A = -2.5$ dB) for the period 23:01–1:06 UT. On 13 December, the nighttime amplitude from 10:23 to 13:54 UT was perceived below the -3σ line and the maximum change in signal amplitude of $\Delta A = -10.7$ dB was measured at 13:09 UT. On 14 December at approximately 6 UT, the system was classified as category 1 TC with a wind speed of 118.5 km/h moving in the northwest direction. Due to change in the intensity and direction towards the receiver, a decline in the amplitude crossing below the -3σ line was observed at 10:25 UT and stabilized with the -3σ line at 13:59 UT, where the most pronounced $\Delta A = -14.3$ dB during the nighttime was measured at 13:21 UT. Again a drop in the daytime amplitude below the -3σ line was sensed from 19:13 to 23:49 UT, where the maximum $\Delta A = -3.1$ dB was recorded at 22:24 UT. TC Yasa completed a loop on 15 December (12:00 UT) and began to move towards Fiji (receiver) at 201.9 km/h. Perturbations in the signal amplitude below -3σ line were observed on 15 to 16 December from 19:13–5:06 UT, where the max. $\Delta A = -5.7$ dB occurred at 4:36 UT. On 16 December, the amplitude anomaly at the nighttime (7:41–11:31 UT) was seen below -3σ line with the maximum $\Delta A = -11.8$ dB at 10:47 UT. At 12:00 UT, category 5 TC Yasa continually moved towards the receiver with a maximum wind speed of ~ 255.6 km/h and the signal amplitude went below the -3σ line at 22:48 UT. The signal amplitude returned to the -3σ line on 17 December at 5:45 UT, where the most pronounced daytime anomaly was observed at 5:44 UT ($\Delta A = -7.4$ dB). At this phase, the movement of TC Yasa was believed to cross Vanua Levu and the TRGCP of the NPM signal to Suva. TC Yasa was still a category 4 cyclone after crossing the second mainland and transmitter–receiver link on 17 December (12:00 UT). VLF signal revealed nighttime amplitudes exceeding below -3σ line (10:27–12:43 UT) with a maximum anomaly observed at 11:07 UT ($\Delta A = -7.7$ dB). On 17 to 18 December, the daytime amplitude decreased below -3σ line (17:37–2:11 UT) with the maximum anomaly at 23:56 UT ($\Delta A = -4.9$ dB). On 18 December, TC Yasa (category 1) moved far from Fiji/VLF receiver in the south path, and the weakening of the TC strength and moving away from the NPM-Suva link showed no anomalies in the VLF propagation from 19 to 21 December. However, the signal amplitude on 22, 23 and 25 December were within the threshold range, most probably due to day-to-day signal variability.

NLK signal amplitude analysis

Similar to Figs. 4, 5 presents the NLK signal amplitude perturbations (panel a-p) during TC Yasa in December 2020 with the diurnal plot of the NLK signal phase on 11 December in panel b. The diurnal amplitude variation in panels (a-p) designates that the signal propagation path is in the complete daylight over 19:00–0:00 UT and complete nighttime over 7:00–16:00 UT. Considering the TD/TC phase of the cyclone, ten clear anomalies were found to cross below -3σ for > 2 h between 11 and 19 December during both the day and night periods of the TRGCP. The first nighttime amplitude anomaly was observed on 11 December from 11:37 to 14:08 UT when the signal went below -3σ line with the maximum $\Delta A = -11.3$ dB at 12:48 UT. The second anomaly was observed on 12 December (12:00 UT) when the TD was approaching Fiji at 64.82 km/h. The amplitude decreased below -3σ line (9:37–14:00 UT), with the maximum $\Delta A = -12.2$ dB at 11:53 UT. On 13 December at 12:00 UT, the TD was heading southeast (away from Fiji) at 83.3 km/h, the amplitude went below -3σ line (11:22–13:41 UT) with the maximum anomaly at 11:33 UT (ΔA = -13.6 dB). On 14 December (~ 6:00 UT), TC Yasa was classified as a category 1 cyclone and the NLK signal amplitude decreased below the -3σ line from 9:42 to 13:36 UT, where the maximum $\Delta A = -15.3$ dB was at 11:54 UT. After completing a loop on 15 December (12:00 UT), TC Yasa moved southwest at 201.9 km/h and the amplitude perturbations went below the -3σ line from 10:12 to 12:47 UT, with a maximum $\Delta A = -11.3$ dB at 4:36 UT. TC Yasa, by now a category 5, continually moved southwest with a maximum wind speed of ~ 255.6 km/h on 16 December (12:00 UT), causing the daytime amplitude to decrease below the -3σ line at 19:19 UT, which recovered to the -3σ line on 17 December at 1:00 UT. A

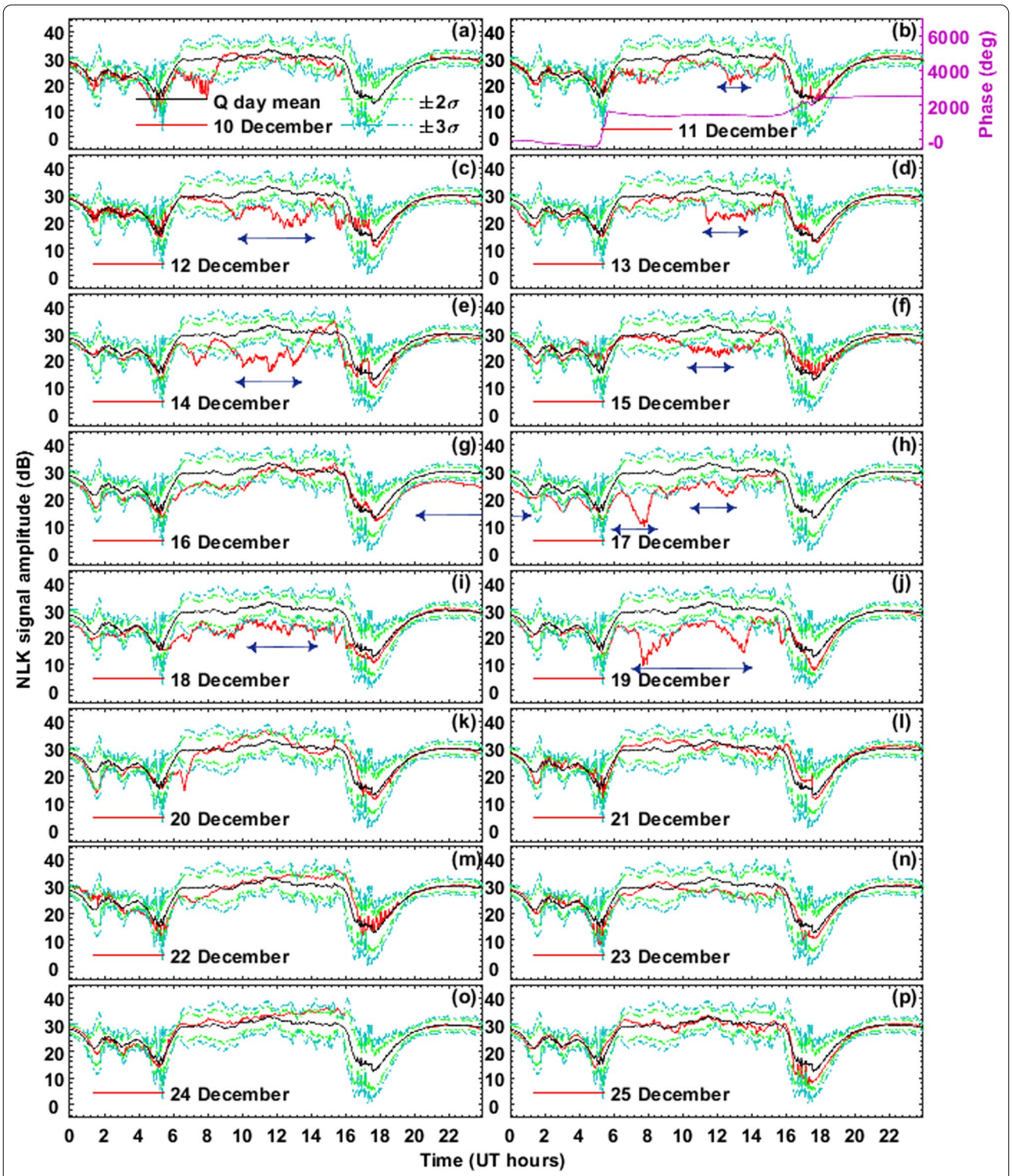

Fig. 5 **a**–**p** NLK signal amplitude (red) during 10 to 25 December 2020 which includes TC Yasa days. The mean signal amplitude for five quiet days (black) along with the ± 2σ (green) and ± 3σ (cyan) are shown. The NLK signal phase on 11 December is shown in purple. Signal amplitude perturbations are marked with blue horizontal arrows

maximum $\Delta A = -5.6$ dB was observed at 23:59 UT. The TC Yasa changed to category 4 while crossing the Vanua Levu and NLK transmitter–receiver link on 17 December (12:00 UT). During this period, the NLK signal exceeded the -3σ line on two nighttime occasions, first between 5:44 and 8:22 UT with a signal amplitude anomaly at 7:47 UT ($\Delta A = -19.8$ dB) and, second between 11:21 and 13:36 UT with the maximum $\Delta A = -10.4$ dB at 12:35 UT. On 18 December at 12:00 UT, TC Yasa was characterized as a category 1 TC as it moved south away from Fiji and later became a TD the following day. A maximum ΔA of -10.9 dB was observed between 10:51 and 12:54 UT on 18 December. On 19 December, the signal exhibited a maximum ΔA of -9.9 dB between 7:14 and 14:01 UT. There were no anomalies present in the VLF propagation from 20 to 25 December because the TC moved away from the sensitive zone and its strength diminished.

JJI signal amplitude analysis

Panels (a–p) in Fig. 6 present the JJI signal amplitude variations during TC Yasa from 10 to 25 December 2020 for complete daylight during 22:00–6:00 UT and complete darkness during 9:00–17:00 UT. The JJI signal phase is not shown because it is completely unstable at our station making it unusable for analysis and modeling. Four anomaly events were observed, three during daytime and one at the nighttime. The first daytime amplitude anomaly occurred on 15 December when TC Yasa was approaching the JJI-Suva link (21:00 UT) in which the signal amplitude decreased below the -3σ line at 23:05 UT and recovered to the -3σ line at 6:26 UT on 16 December, where maximum $\Delta A = -4.3$ dB was observed at 1:45 UT. Later into the day at 21:00 UT, TC Yasa intensified into a category 4 cyclone and began approaching the Suva receiver with wind speed of ~ 242.6 km/h. This coincided with a decrease in the signal amplitude below the -3σ line at 22:32 UT and recovered to the -3σ line on 17 December at 6:26 UT. The maximum anomaly was observed at 1:35 UT with $\Delta A = -4.8$ dB. On 17 to 18 December, a signal amplitude anomaly occurred during 22:40–5:20 UT with maximum $\Delta A = -4.1$ dB at 22:56 UT. The anomaly at the nighttime was observed above the $+3\sigma$ line for ~ 2 h with a maximum $\Delta A = 4.6$ dB at 13:02 UT. Later, the system was classified as a TD and began moving south away from the Suva receiver. No TC-related perturbations were observed from 19 to 21 December.

Figure 7 shows the *Dst* and *Kp* index during TC Yasa, revealing quiet *Dst* values varying above -22 nT and *Kp* values below 4 in December 2020 (http://wdc.kugi.kyoto-u.ac.jp/dst_realtime/202012/index.html). B-class solar flares were observed during the 10 to 25 December and a C 4.3-class flare occurred at 14:35 UT on 14 December 2020 (https://www.spaceweatherlive.com/en/archive.html) at the nighttime of the TRGCPs indicating no solar flare effect during the TC.

D-region perturbations during TC Yasa: LWPC modeling

To determine the perturbed values of the Wait parameters; the reference height H' and sharpness factor β for each perturbation event, we first ran the LWPC code (V2.1) to obtain their ambient (unperturbed) values along the NPM signal path using the coordinates of the NPM transmitter and the Suva receiver (latitude and longitude) and the date and time (in UT) of the perturbation event. The ambient values obtained are assumed to be constant along the NPM signal propagation path except in the perturbed segment. This estimation of the unperturbed values of the Wait parameters is similar to the approach used by Kumar et al. (2017) and Pal et al. (2020). The values of H' and β were then varied from their unperturbed values until the modeled signal closely matched the real-time signal based on the magnitude of the maximum perturbation in the signal amplitude or amplitude and phase both. The resulting H' and β are identified as the perturbed values associated with the perturbed segment of the NPM signal path and are considered to vary as a Gaussian that extends up to 1000 km in either direction from the projected position of the TC eye on the signal path. A detailed explanation of this procedure can be further found in the work by NaitAmor et al. (2017). Figure 8 shows the results of the LWPC modeling of four clear NPM signal perturbation events (two daytime and two nighttime) selected from Fig. 4. The four perturbation events modeled exhibited amplitudes exceeding the -3σ line for at least 2 h. Modeling of the two daytime signal perturbation events resulted in the unperturbed values of $H' = 74$ km and $\beta = 0.30$ km^{-1}. An increase in the H' and a decrease in the β by 10.6 km and 0.143 km^{-1}, respectively, were estimated for the daytime signal perturbation event on 13 December at 0:46 UT (panel a), whereas an increase in both H' and β by 9.7 km and 0.143 km^{-1}, respectively, were observed for the daytime signal perturbation on 14 December at 22:23 UT (panel b). Interestingly, the outer and inner rainband lightnings reached a local peak prior to the perturbations in the daytime H' and β as can be seen in Fig. 3. Applying the same modeling used in the daytime perturbations to the nighttime perturbations, the nighttime unperturbed values of $H' = 87$ km and $\beta = 0.43$ km^{-1} were obtained. Compared to the daytime perturbations, both H' and β for the two nighttime perturbation events considered decreased from their unperturbed values. For the signal perturbation on 16 December at 10:47 UT (panel c), H' decreased by

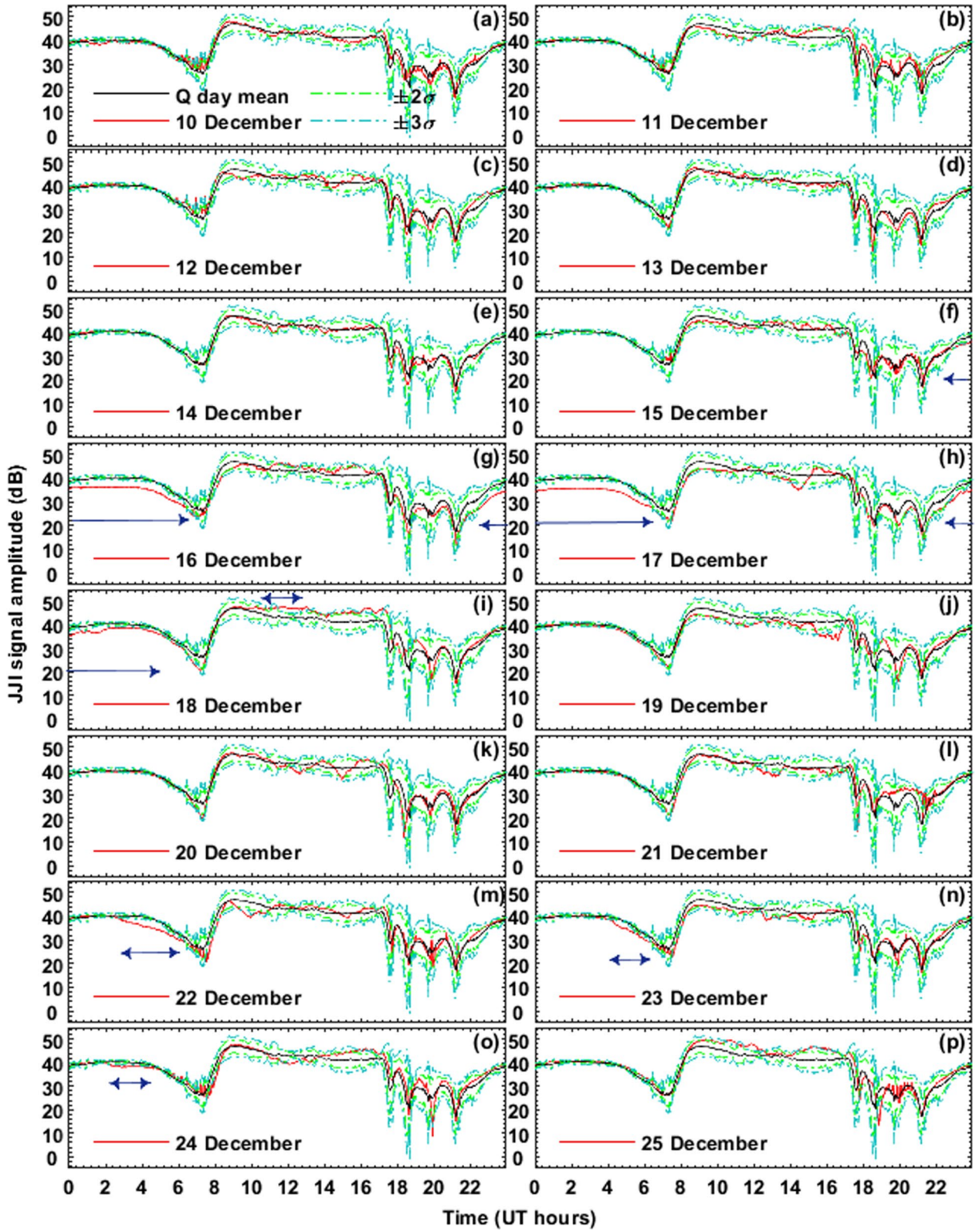

Fig. 6 **a**–**p** JJI signal amplitude (red) during 10 to 25 December 2020 which includes TC Yasa days. The mean signal amplitude for five quiet days (black) along with the ± 2σ (green) and ± 3σ (cyan) are shown. Signal amplitude perturbations are marked with blue horizontal arrows

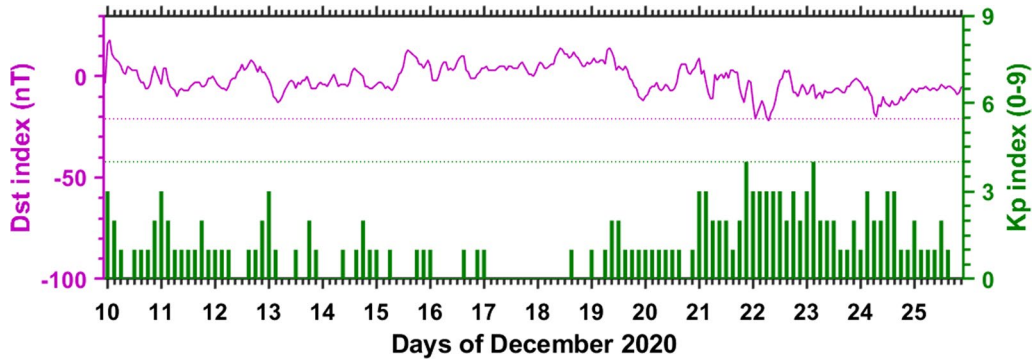

Fig. 7 *Dst* (purple) and *Kp* (green) indices during during 10 to 25 December 2020 which includes TC Yasa days

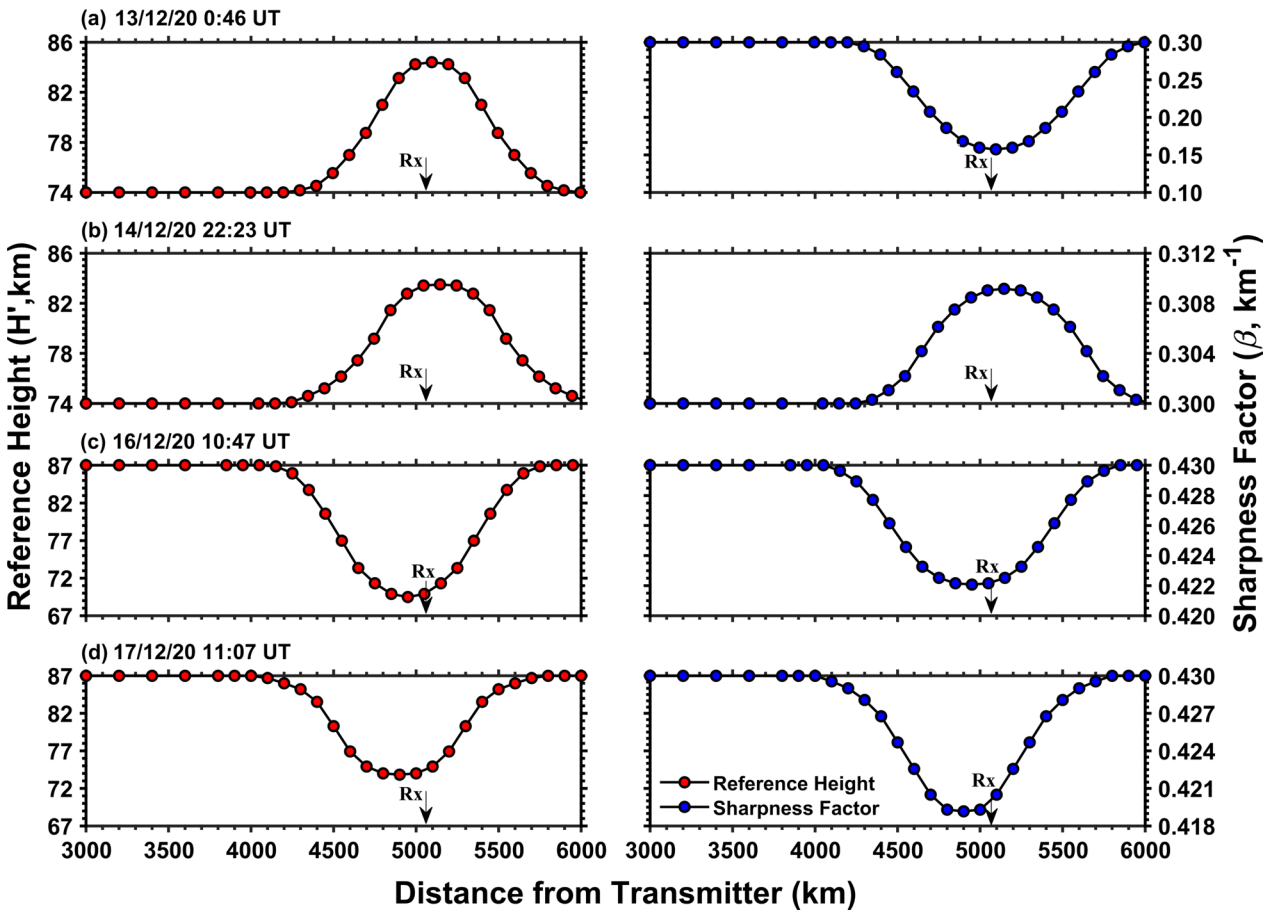

Fig. 8 The variation of ionospheric Wait parameters, H' (first column, red) and β (second column, blue), based on the LWPC modeling of the following NPM signal perturbations: the daytime signal perturbations on a 13 December 2020 at 0:46 UT and b 14 December 2020 at 22:23 UT and the nighttime signal perturbations on c 16 December 2020 at 10:47 UT and d 17 December 2020 at 11:07 UT. The relative distance of the Suva receiver (Rx) from the NPM transmitter is indicated by the arrow pointing downwards

17.7 km while β decreased by 0.008 km^{-1}, whereas for the signal perturbation on 17 December at 11:07 UT (panel d), H' decreased by 13.2 km while β decreased by 0.011 km^{-1}. Notable local peaks in lightning activity can again be seen, in the eyewall region in this case, prior to the two nighttime VLF perturbation events in

H' and β. Three more events (1 daytime and 2 nighttime) events were modeled using the LWPC code. Tables 1 and 2 provide a summary of the changes in Wait parameters associated with all seven selected events. It can be observed that the perturbed H' is more visible at night as compared to the day. In addition, we have further analyzed and determined the temporal changes (hourly) of the associated Wait parameters using LWPC modeling of a daytime NPM signal perturbation from 17 December at 18:00 UT to 18 December at 6:00 UT and is given in Fig. 9. The time interval chosen covers the period that starts at the end of the sunrise terminator and finishes at the beginning of the sunset terminator. From the plots, wave-like variation of both Wait parameters (H' and β) may be attributed to the influence of propagating GWs from below, reaching up to D-region ionospheric heights.

Gravity waves associated with TC Yasa: wavelet analysis

After analyzing the ionospheric high frequency Doppler shift data recorded at a station in Peking University during 24 typhoons from 1987 to 1992, Xiao et al. (2007) suggested that the corresponding changes in the lower ionosphere and electron content may be attributed to the influence of AGWs produced by the typhoons. To determine the TC-induced WLS present in the perturbed

Table 1 The signal characteristic and D-region parameters for three daytime NPM signal anomaly events

No. of events	Date (dd/mm/yy)	Time (hh:mm UT)	ΔAmplitude (dB)	Δφ (deg)	ΔH' (km)	Δβ (km^{-1})
1	13/12/20	00:46	− 2.278	+ 12	+ 10.6	− 0.143
2	14/12/20	22:23	− 3.081	− 90	+ 9.7	+ 0.010
3	16/12/20	02:36	− 5.669	− 100	+ 10.6	+ 0.005

Table 2 The signal characteristic and D-region parameters for four nighttime NPM signal anomaly events

No. of events	Date (dd/mm/yy)	Time (hh:mm UT)	ΔAmplitude (dB)	Δφ (deg)	ΔH' (km)	Δβ (km^{-1})
1	13/12/20	13:09	− 10.664	+ 97	− 18.0	− 0.070
2	14/12/20	13:25	− 14.297	+ 148	− 19.2	− 0.050
3	16/12/20	10:47	− 11.831	+ 137	− 17.7	− 0.008
4	17/12/20	11:07	− 7.710	+ 100	− 13.2	− 0.011

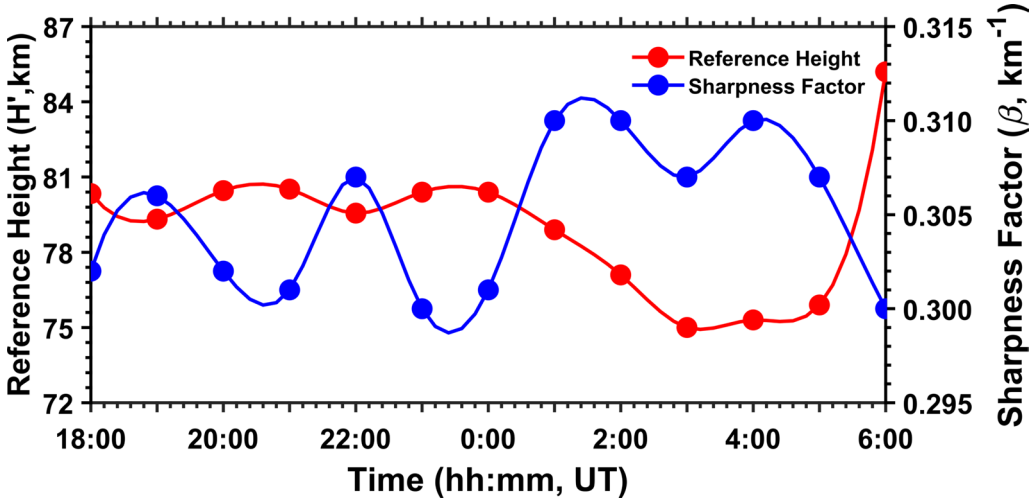

Fig. 9 Temporal variation of the ionospheric Wait parameters, H' (red) and β (blue), associated with the daytime NPM signal perturbation detected on 17 December 2020 at 18:00 UT to 18 December at 6:00 UT during TC Yasa

signals, the reduced amplitudes (ΔA) of the NPM, NLK, and JJI signals were used in the wavelet analysis to minimize and remove any diurnal variability in the signals. In doing so, the signals are expected to be free from variable influences induced by other sources such as topographic effects and auroral quasi-periodic oscillations (Boška and Laštovicka 1996; Laštovička 2006) apart from waves associated with solar terminator (Nina and Čadež 2013). Figure 10 presents the spectrums of the NPM, NLK, and JJI signals during TC Yasa from 10 to 25 December 2020 based on the wavelet analysis for separate daytime (left column) and nighttime (right column) periods. The x-axis represents the days of the month and the y-axis shows the frequency ranging from 0.05 to 0.65 mHz. Enhanced amplitudes of WLS at frequencies of 0.05–0.07 mHz corresponding to periods of 3.9–5.5 h can be observed from 14 to 19 December in the daytime spectra of both the NPM (panel a, 20:00–3:00 UT) and NLK (panel c, 19:00–0:00 UT) signals and from 11 to 12 December in the daytime spectra of the JJI (panel e, 22:00–6:00 UT) signal. An increase in WLS amplitude can also be observed from 21 to 23 December in the JJI daytime spectrum but this may not be relevant to TC Yasa which dissipated by 19 December. For the nighttime spectra, a notable increase in the amplitudes for WLS in the frequency range of 0.05–0.10 mHz corresponding to periods of 2.7–5.5 h can be observed for all three signals. For the NPM signal (panel b, 7:00–16:00 UT), the nighttime WLS occurred on 10 and 15 to 19 December, while for the NLK signal (panel d, 7:00–16:00 UT), the nighttime WLS occurred on 10 and 16 to 18 December. The nighttime WLS in the JJI signal (panel f, 9:00–17:00 UT) similarly occurred between 16 and 18 December. Interestingly, the occurrence times of the enhancement in WLS amplitudes during both daytime and nighttime coincide with the periods when TC Yasa was developing into a TD (10–13 December) and when TC Yasa reached its peak intensity (15–16 December). Additionally, the amplitudes of the WLS in all the three signals during nighttime are observed to be comparatively higher than those during daytime.

Discussion

Lightning occurrence during TC Yasa

Lightning is one of the characteristic phenomena in the convective cloud systems. Lightning strokes can be treated as indicators to detect the presence of significant convection (Molinari et al. 1999) and the intensity of convection within convective storms (MacGorman and Morgenstern 1998). Monitoring of lightning within storms has since been studied as a feasible way of possibly forecasting storm intensification (Demaria et al. 2012; Molinari et al. 1994; Solorzano et al. 2008). At the same time, convective activity is considered as one of the dominant sources of GWs, particularly in the tropics where TCs are known to be the strongest convective storms (Fritts and Alexander 2003). The analysis of WWLLN lightning location data during TC Yasa indicated the enhanced lightning activity and, hence, convective activity in all three regions of TC Yasa near or within the sensitive zones of the NPM, NLK, and JJI transmitter links. Of the three regions, the outer rainband showed the highest convective activity which

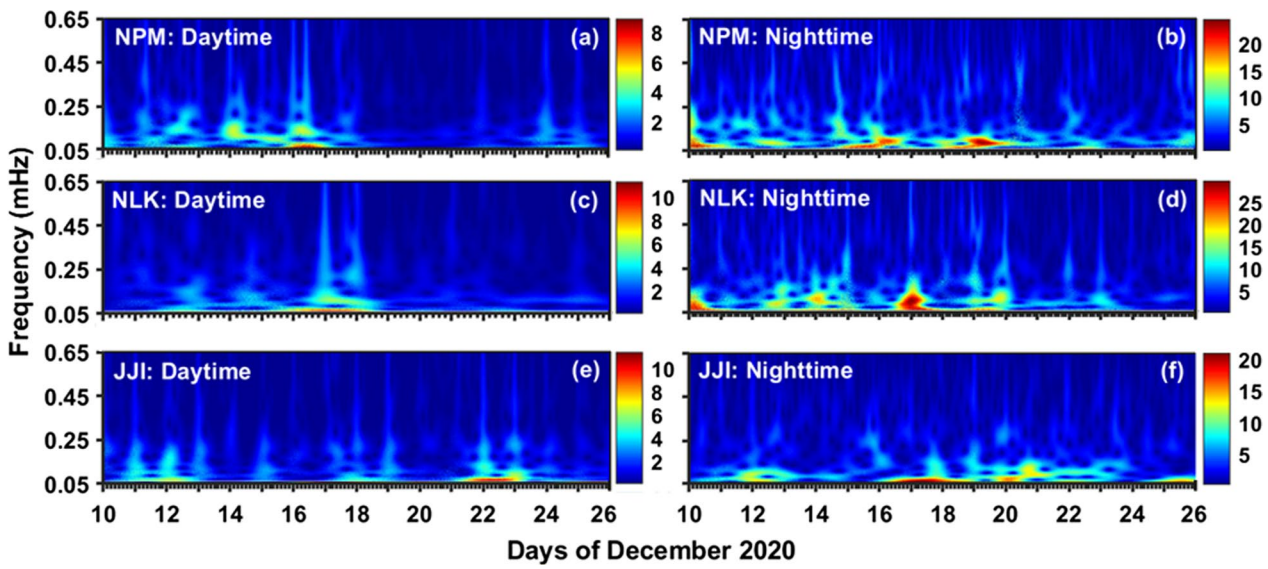

Fig. 10 The mother Morlet wavelet spectra of NPM (**a**, **b**), NLK (**c**, **d**) and JJI (**e**, **f**) signals during 10 to 25 December 2020. The daytime and nighttime spectra for each signals are shown in the left and right columns, respectively

was reflected in terms of the high number of lightning events for a large number of days compared to the eyewall and inner rainband. It can be inferred that the high convective activity in the outer rainband may be the likely meteorological source of AGWs within TCs that potentially disturbs the lower ionosphere. However, it should be pointed out that our results do not rule out the possibility that GWs are also generated in the eyewall and inner rainband but merely suggests that the majority of the waves may have originated in the outer rainband. Moreover, by comparing the lightning data surrounding TC Yasa against the storm's maximum sustained winds, it was determined that there are multiple peaks in the total lightning activity throughout the storm's lifetime with the maximum peak in total lightning activity preceding the peak of the maximum sustained winds for a day (24 h). An interesting observation is that the maximum peak in total lightning activity corresponds to the peak in lightning activity of the outer rainband. In comparison, the peaks in lightning activity for the eyewall and inner rainband occurred for several hours and days, respectively, after the peak in maximum sustained winds or during the weakening phase of TC Yasa. Our results showed that lightning activity peaked before TC Yasa reached its highest intensity based on maximum sustained winds and that this peak in lightning activity is attributed to lightning in the outer rainband of the TC. This is consistent with the work by Demaria et al. (2012) where authors examined the lightning activity associated with TCs in the Atlantic and eastern North Pacific from 2005 to 2010 and observed high lightning density in the rainband regions (200–300 km) of cyclones that rapidly intensified 24 h. Demaria et al. (2012) also observed high lightning density in the inner-core of TCs that rapidly weakened and suggested that inner-core lightning outbreaks signaled the end of the intensification phase. This is in agreement with our results showing a peak in the eyewall lightning activity several hours into the weakening phase of TC Yasa. Xu et al. (2017) made similar findings after examining TCs in six TC-prone basins and determined that intensifying TCs showed significantly low inner core (0–100 km) and high outer rainband (200–400 km) lightning density compared to weakening and neutral TCs where the lightning density in the inner core and outer rainbands were high and low, respectively. The eyewall lightning outbreak during the weakening phase of TCs can be explained by the interaction between the inner core potential vorticity and incident vertical wind shear as determined by Davis et al. (2008) after conducting simulations of six Atlantic hurricanes. Davis et al. (2008) showed that the wind shear tilts the inner core potential vorticity resulting in asymmetric but intense convection.

VLF perturbations and D-region changes associated with TC Yasa

Upon analyzing the VLF signals received from the NPM, NLK, and JJI transmitters during TC Yasa, we have identified significant signal anomalies associated with the intensification and weakening of the TC where all the three signals showed strong perturbations beyond -3σ level (negative anomalies) lasting for at least 2 h or more. Of the three signals, the JJI signal also showed a signal perturbation above the $+3\sigma$ level (positive anomaly) lasting for ~ 2 h. The negative and positive signal amplitude anomalies can be explained in terms of destructive and constructive interference between the modes reflected from disturbed region and normal segments of the waveguide (direct mode). For the NPM-Suva path, only daytime anomalies were observed when the TD moved towards the TRGCP, and a stable daytime signal was recorded when the cyclone was a category 1 and was situated 317.8 km near the VLF receiving station. Both daytime and nighttime anomalies were revealed on the NLK-Suva link which commenced when the TD was located 769.3 km west of the TRGCP and the anomalies vanished after the TC crossed the TRGCP and weakened back to the TD about 611.9 km south of the receiver. Again, both daytime and nighttime perturbations on the JJI-Suva path began when the category 5 system set 110.3 km west beside the JJI-Suva path and the anomalies faded upon category 1 classification about 359.7 km south of the receiving station. The most significant perturbations were observed when the storm approached the transmitter–receiver path or the sensitive area, i.e., during daytime for NPM, $\Delta A = -7.4$ dB and for JJI, $\Delta A = -4.8$ dB, whereas at the nighttime for NLK, $\Delta A = -19.8$ dB. Our results show that signal amplitude anomalies can occur both during the daytime and nighttime. In our case, mostly the negative anomalies were observed (one positive anomaly from JJI-Suva link on 18 Dec 2020, see Fig. 6, panel i) and the negative and positive perturbations are mainly due to the propagating distance of the received signal (NaitAmor et al. 2017) and distance between the storm to GCP which causes the constructive or destructive modal interference at the receiver resulting in negative or positive anomaly (NaitAmor et al. 2018). Equivalent to our case, Kumar et al. (2017) observed negative daytime and nighttime anomalies in the NPM, NLK, and JJI signal amplitude when the TC Evan was inside the sensitive zone. Interestingly, our results revealed clear daytime perturbations with periods between 2 and 9 h in

NPM-Suva signal path, 2–6 h in NLK-Suva signal path, and 2–7 h in JJI-Suva signal path while a clear nighttime perturbation of 2–4 h in NLK-Suva signal path with different magnitude and the signal amplitude perturbations beyond -3σ mark.

We have used the LWPC v2.1 code to model TC-induced perturbations in the NPM signal observed during TC Yasa to estimate the associated disturbance in the lower ionosphere in terms of changes to the, H', and and β. The LWPC code has been used similarly in past research of the lower ionosphere which involved establishing parameters that characterize the region during daytime and nighttime conditions (Thomson et al. 2007, 2011) and during times of perturbed conditions associated with geomagnetic storms (Kumar et al. 2015), lightning-induced electron precipitations (Poulsen et al. 1993), solar eclipses (Clilverd et al. 2001), solar flares (Thomson et al. 2005), and transient luminous events (NaitAmor et al. 2017). More recently, it was used to investigate ionospheric signatures of possible TC–ionosphere coupling where upward propagating GWs were suggested as the causes of the ionospheric disturbances (Bakul et al. 2021; Kumar et al. 2017). The results of our attempt to model the response of the lower ionosphere region in terms of estimated changes to H' and β with reference to their unperturbed values show that the behavior of the region is different during daytime and nighttime perturbations. For daytime perturbations, H' was observed to increase while β exhibited both increase and decrease, whereas for nighttime perturbations, both H' and β decreased. Moreover, a significant change in reference height, $\Delta H'$, with an appreciably small change in sharpness factor, $\Delta\beta$, was estimated from modeling of the daytime and nighttime signal perturbations. The changes in the reference height may be attributed to the motion induced by the propagation of upward GWs (Marshall and Snively 2014) which lifts and sinks the background atmosphere and drags the D-region ionization with it given that the cyclone does not alter the source and loss mechanism of the lower ionosphere region. The largest changes in the daytime Wait parameters were $\Delta H' = +10.6$ km and $\Delta\beta = -0.143$ km^{-1}, whereas the largest changes to the nighttime parameters were $\Delta H' = -19.2$ km and $\Delta\beta = -0.050$ km^{-1}, indicating stronger D-region TC effect at the nighttime as compared to the daytime. In comparison, Kumar et al. (2017) reported a maximum decrease of ~ 5.2 km in the nighttime D-region H' and a maximum increase of 7.2 km in daytime D-region H' after studying the perturbations of local origin in VLF signals of NPM, NLK, NAA, and JJI transmitters during TC Evan in the South Pacific. Bakul et al. (2021) also determined a maximum decrease in the H' of the nighttime D-region by ~ 7.9 km after modeling the perturbations in VTX, NWC, and JJI signals recorded at two receiving stations (Kolkata and Cooch Behar, India) during TC Fani in the North Indian Ocean. Ionospheric fluctuations in the D-region height were similarly found by Lay and Shao (2011) after carrying out a multi-station time-domain analysis of lightning waveforms associated with a large thunderstorm on 17 June 2005. The authors showed that the nighttime perturbations to the D-region height can on average reach about 6 km due to the AGWs that arise from the convective storms overshooting the tropopause and disturbing the lower ionosphere. Our results for TC Yasa corroborates the findings of the studies above and show the stronger lower ionosphere perturbations particularly at the nighttime which can be associated with the susceptibility of the lower ionosphere to the meteorological influences from below in the absence of incident solar radiation at night.

The AGWs act as a carrier for the tropospheric disturbances to the ionosphere (Pal et al. 2020). A TD or TC perturbs the particles in the atmosphere from their equilibrium state and the gravity force pulls those particles back to the equilibrium. Due to this, non-stationary atmospheric GWs having horizontal wavelength ranging from several tens to several thousands of kilometer and vertical wavelength varying 1–6 km are generated which propagate through the troposphere and affect the mesosphere and lower ionosphere (Das et al. 2012). The sources for AGWs have been proposed to be largely from upward propagating meteorological processes (convention activity in the troposphere and stratosphere). AGWs could be driven by wind component along the magnetic field direction or through longitudinal mobility which are indirectly generated via convergence–divergence of ionization (MacDougall et al. 2009). It can also be produced by the sunrise and sunset terminators or seeded by the intertropical convergence zone (MacDougall et al. 2011). According to Vadas et al. (2009), deep clouds near the tropopause are evidence of regions of active convection and the likely source of GWs. AGWs generated from the convective system can propagate into higher altitudes and penetrate deep into the atmosphere (Yigit et al. 2008), and can produce variation in the VLF signal during daytime and nighttime when TC crosses the transmitter–receiver path (Pal et al. 2020; NaitAmor et al. 2018). The amplitude and phase of the VLF signals propagating in EIWG are affected by the conditions of the local electron density at the VLF reflection height in the D-region. The spatial modulations produced by the GWs in the neutral density produce changes in the electrical conductivity of the

D-region and cause variations in the VLF signal. We used Morlet wavelet analysis to three VLF transmitter signals amplitude to examine wave-like spectra during day and night periods and found a clear transition from quiet days to TD/TC disturbed days with wave-like spectra associated with GWs. All the three transmitters had daytime wave-like events with periods between 3.9 and 5.5 h when the TC approached the paths, while NPM, NLK, and JJI had nighttime wave-like events with periods starting from 2.2, 2.1, and 3.9 to 5.5 h, respectively. Consistent with the findings of Kumar et al. (2017), we found similar signal spectrums for NPM and NLK signals, which could be due to their paths being close to each other. NaitAmor et al. (2018) studied VLF signal anomalies from August to November 2016 cyclones in the Atlantic Ocean using mother wavelet analysis of normalized signal amplitude and found nighttime wave-like events with periods between 2 and 3 h. Pal et al. (2020) applied the wavelet analysis method to the residual perturbed VTX signal amplitude from the severe cyclone Fani of May 2019 and confirmed the major enhancement of AGWs spectrum with periods 10 min to 2 h during landfall. Our outcomes correlate with these studies and show that wave-like oscillations of wider periods could be related to TCs.

We found that the perturbations occurred when the low-pressure system was still a TD and when it strengthened into a TC. The perturbations were assumed to originate from TC Yasa because there were no geomagnetic storms or solar flares of class C and above during the TC Yasa. Moreover, there were no other TCs crossing the NPM/NLK/JJI-Suva GCP from 10 to 25 December 2020. The signal perturbations observed from 10 to 11 December may be attributed to the early formation of TC Yasa which is consistent with the findings of Nina et al. (2017) who identified VLF signal perturbations during the early beginnings of TCs. A total of six earthquakes occurred within the wave-sensitive area of the TRGCPs, i.e., within the fifth Fresnel zone during the period of TC Yasa. Using all known methods (Kumar et al. 2013), initial checks for any seismo-ionospheric signatures on the VLF signals were made. All the earthquakes were below magnitude 5, and hence their effect on the VLF propagation and D-region ionosphere could not be seen and are unlikely to occur. However, the days from 22 to 24 December 2020 showed negative perturbations for more than 2 h outside the TC period which included geomagnetically disturbed days (21–24 December). The significant anomalies outside the TC period were possibly due to forcing from auroral region because TIDs are known to be the indicator of the AGWs arising either from the underlying troposphere or from the auroral region (Hunsucker 1982; Huang et al. 1994; Miller et al. 1997) or of the local origin. Such anomalies are rarely observed.

Summary and conclusions

It is evident from our results that there is a strong connection between the lightning activity (convective activity) and the observed perturbations in the VLF signals due to the D-region changes (parameters H' and β) during the TC Yasa. WWLLN lightning data during TC Yasa revealed enhanced lightning activity in all three regions of the TC that are observed to fall near or within the sensitive zones of the NPM, NLK, and JJI transmitter–receiver paths. Of the three regions, the outer rainbands showed the highest density of lightning activity, but each region showed distinct lightning evolution during different times of the TC which were observed to closely follow the detected VLF signal perturbations. Our VLF signal analysis showed both positive and negative signal perturbations both during daytime and nighttime with the change in signal amplitudes from the quiet baseline values determined to reach up to −4.9dB(JJI) during the day and −19.8dB(NLK) during the night. Additionally, VLF signal perturbations with long occurrence times were also determined during daytime (~ 2–9 h) and nighttime (~ 2–7 h). From the LWPC modeling of the NPM signal having a purely low-latitude path, the response of the lower D-region ionosphere for daytime perturbations showed an increase in the H' and both increase and decrease in β, whereas for nighttime perturbations, both H' and β decreased. The largest changes in the daytime Wait parameters were $\Delta H' = +10.6$ km and $\Delta\beta = -0.143$ km^{-1}, whereas the largest changes in the nighttime parameters were $\Delta H' = -19.2$ km and $\Delta\beta = -0.050$ km^{-1}. Finally, based on the mother Morlet wavelet analysis of the three VLF transmitter signals during the day and night periods, we found a clear transition of WLS from quiet days to TC disturbed days with the periods of the WLS in agreement with those of gravity waves. Daytime WLS with periods between 3.9 and 5.5 h and nighttime WLS with periods between 2.1 and 5.5 h were observed in all the spectrums of the three VLF signals.

Abbreviations

AGWs: Atmospheric gravity waves; EIWG: Earth-ionosphere waveguide; Dst: Disturbance storm time; LWPC: Long Wavelength Propagation Capability; NOAA: National Oceanic and Atmospheric Administration; PICs: Pacific Island Countries; Q-days: Quiet days; TCs: Tropical cyclones; TDs: Tropical depressions; TIDs: Travelling ionospheric disturbances; TRGCPs: Transmitter–receiver great circle paths; VLF: Very low frequency; WLS: Wave-like signatures; WWLLN: Worldwide Lightning Location Network.

Acknowledgements

Not applicable.

Author contributions

The authors PAALR and SK_1 analyzed the lightning and VLF data for TC effects on VLF and carried out the D-region modeling in consultation with AK and

SK_2. The manuscript was jointly prepared by PAALR, SK_1, AK and SK_2. All authors read and approved the final manuscript.

Funding
The authors are thankful for the financial support by The University of the South Pacific's main research office under the Strategic Research Theme (Grant No. F7304-RI001-ACC-001) under which this work has been carried out.

Availability of data and materials
The VLF data are available with PAALR and SK. The lightning data were obtained from the WWLLN database (WWNNL, http://wwlln.net/) which is a global lightning location detection network, while the wind speed data were obtained from National Oceanic and Atmospheric Administration (NOAA), https://www.ncei.noaa.gov/access/monitoring/monthly-report/tropicalcyclones/202013). The five Q-days were obtained from the World Data Centre website http://wdc.kugi.kyoto-u.ac.jp/.

Declarations

Competing interests
The authors declare that they have no competing interests.

Received: 12 November 2021 Accepted: 14 April 2022
Published online: 28 April 2022

References

Abarca SF, Corbosiero KL, Galarneau TJ (2010) An evaluation of the Worldwide Lightning Location Network (WWLLN) using the National Lightning Detection Network (NLDN) as ground truth. J Geophys Res 115:D18206. https://doi.org/10.1029/2009JD013411
Addison PS (2017) The illustrated wavelet transform handbook: introductory theory and applications in science, engineering, medicine and finance, 2nd edn. CRC Press, Boca Raton
Ávila EE, Bürgesser RE, Castellano NE, Collier AB, Compagnucci RH, Hughes RW (2010) Correlations between deep convection and lightning activity on a global scale. J Atmos Sol Terr Phys 72(14):1114–1121. https://doi.org/10.1016/j.jastp.2010.07.019
Bakul D, Shubham S, Kumar HP, Kumar MS, Sujay P (2021) D-region ionospheric disturbances associated with the Extremely Severe Cyclone Fani over North Indian Ocean as observed from two tropical VLF stations. Adv Space Res 67(1):75–86. https://doi.org/10.1016/j.asr.2020.09.018
Bauer SJ (1958) An apparent ionospheric response to the passage of hurricanes. J Geophys Res Space Phys 63(1):265–269. https://doi.org/10.1029/JZ063i001p00265
Boška J, Laštovicka J (1996) Gravity wave activity in the lower ionosphere and in the F2 region—Similarities and differences. Adv Space Res 18(3):127–130. https://doi.org/10.1016/0273-1177(95)00851-5
Bürgesser RE (2017) Assessment of the World Wide Lightning Location Network (WWLLN) detection efficiency by comparison to the Lightning Imaging Sensor (LIS). QJR Meteorol Soc 143(708):2809–2817. https://doi.org/10.1002/qj.3129
Choudhury A, De BK, Guha A, Roy R (2015) Long-duration geomagnetic storm effects on the D region of the ionosphere: some case studies using VLF signal. J Geophys Res Space Phys 120(1):778–787. https://doi.org/10.1002/2014JA020738
Clilverd M, Rodger C, Thomson N, Lichtenberger J, Steinbach P, Cannon P, Angling M (2001) Total solar eclipse effects on VLF signals: observations and modeling. Radio Sci 36:773–788. https://doi.org/10.1029/2000RS002395
Crombie DD (1964) Periodic fading of VLF signals received over long paths during sunrise and sunset. Radio Sci 68D(1):27–34
Das SS, Uma K, Das SK (2012) MST radar observations of short-period gravity wave during overhead tropical cyclone. Radio Sci 47(02):1–10. https://doi.org/10.1029/2011RS004840
Das B, Sarkar S, Haldar PK, Midya SK, Pal S (2021) D-region ionospheric disturbances associated with the Extremely Severe Cyclone Fani over North Indian Ocean as observed from two tropical VLF stations. Adv Space Res 67(1):75–86. https://doi.org/10.1016/j.asr.2020.09.018
Davis CA, Jones SC, Riemer M (2008) Hurricane vortex dynamics during Atlantic extratropical transition. J Atmos Sci 65(3):714–736. https://doi.org/10.1175/2007jas2488.1
Demaria M, Demaria R, Knaff J, Molenar D (2012) Tropical cyclone lightning and rapid intensity change. Mon Weather Rev 140:1828–1842. https://doi.org/10.1175/MWR-D-11-00236.1
Dowden, RL, Adams CDD (2008) SoftPAL, Proceedings of the 3rd VERSIM Workshop, Tihany, Hungary, 15–20 Sept. 2008.
Ferguson J A (1998) Computer programs for assessment of long-wavelength radio communications, Version 2.0., Technical document 3030. Space and Naval Warfare Systems Center, San Diego
Fritts DC, Alexander MJ (2003) Gravity wave dynamics and effects in the middle atmosphere. Rev Geophys 41(1):1003. https://doi.org/10.1029/2001rg000106
Hayakawa M (2015) Earthquake prediction with radio techniques. Wiley, Hoboken
Holzworth RH, McCarthy MP, Brundell JB, Jacobson AR, Rodger CJ (2019) Global distribution of superbolts. J Geophys Res Atmos 124(17–18):9996–10005. https://doi.org/10.1029/2019JD030975
Huang CS, Miller CA, Kelley MC (1994) Basic properties and gravity wave initiation of the midlatitude F region instability. Radio Sci 29:395–405. https://doi.org/10.1029/93RS01669
Huang C-M, Richmond AD, Chen M-Q (2005) Theoretical effects of geomagnetic activity on low-latitude ionospheric electric fields. J Geophys Res 110(A5):A05312. https://doi.org/10.1029/2004JA010994
Hunsucker RD (1982) Atmospheric gravity waves generated in the high-latitude ionosphere: a review. Revs Geophys 20(2):293–315. https://doi.org/10.1029/RG020i002p00293
Hutchins ML, Holzworth RH, Rodger CJ, Brundell JB (2012) Far-field power of lightning strokes as measured by the world wide lightning location network. J Atmos Oceanic Tech 29(8):1102–1110. https://doi.org/10.1175/jtech-d-11-00174.1
Isaev N, Sorokin V, Chmyrev V, Serebryakova O, Yashchenko A (2002) Disturbance of the electric field in the ionosphere by sea storms and typhoons. Cosm Res 40(6):547–553. https://doi.org/10.1023/A:1021549612290
Kerrache F, NaitAmor S, Kumar S (2021) Ionospheric D region disturbances due to FAC and LEP associated with three severe geomagnetic storms as observed by VLF signals. J Geophys Res Space Physics 126:e2020JA027838. https://doi.org/10.1029/2020JA027838
Kumar A, Kumar S (2020) Ionospheric D region parameters obtained using VLF measurements in the South Pacific region. J Geophys Res: Space Phys 125(1):e2019JA027536. https://doi.org/10.1029/2019JA027536
Kumar S, Kumar A, Rodger CJ (2008) Subionospheric early VLF perturbations observed at Suva: VLF detection of red sprites in the day? J Geophys Res 113(A3):A03311. https://doi.org/10.1029/2007JA012734
Kumar A, Kumar S, Hayakawa M, Menk F (2013) Subionospheric VLF perturbations observed at low latitude associated with earthquake from Indonesia region. J Atmos Sol-Terr Phys 102:71–80. https://doi.org/10.1016/j.jastp.2013.04.011
Kumar S, Kumar A, Menk F, Maurya AK, Singh R, Veenadhari B (2015) Response of the low-latitude D region ionosphere to extreme space weather event of 14–16 December 2006. J Geophys Res Space Phys 120(1):788–799. https://doi.org/10.1002/2014JA020751
Kumar S, NaitAmor S, Chanrion O, Neubert T (2017) Perturbations to the lower ionosphere by tropical cyclone Evan in the South Pacific Region. J Geophys Res Space Phys 122(8):8720–8732. https://doi.org/10.1002/2017ja024023
Laštovička J (2006) Forcing of the ionosphere by waves from below. J Atmos and Sol-Terr Phys 68(3–5):479–497. https://doi.org/10.1016/j.jastp.2005.01.018
Lay EH, Shao X-M (2011) Multi-station probing of thunderstorm-generated D-layer fluctuations by using time-domain lightning waveforms. Geophys Res Letts 38(23):L23806. https://doi.org/10.1029/2011gl049790
MacDougall JW, Li G, Jayachandran PT (2009) Traveling ionospheric disturbances near London, Canada. J Atmosc and Sol-TerrPhys 71(17–18):2077–2084. https://doi.org/10.1016/j.jastp.2009.09.016
MacDougall JW, Abdu MA, Batista I, Buriti R, Medeiros AF, Jayachandran PT, Borba G (2011) Spaced transmitter measurements of medium scale

traveling ionospheric disturbance near equator. Geophys Res Letts 38(16):L16806. https://doi.org/10.1029/2011GL048598
MacGorman DR, Morgenstern CD (1998) Some characteristics of cloud-to-ground lightning in mesoscale convective systems. J Geophys Res 103(D12):14011–14023. https://doi.org/10.1029/97JD03221
Mallat S (1999) A wavelet tour of signal processing. Elsevier, Hoboken
Marshall RA, Snively JB (2014) Very low frequency subionospheric remote sensing of thunderstorm-driven acoustic waves in the lower ionosphere. J Geophys Res Atmos 119(9):5037–5045.
Miller CA, Swartz WE, Kelley MC, Mendillo M, Nottingham D, Scali J, and Reinisch B (1997) Electrodynamics of midlatitude spread F:1. Observations of unstable, gravity wave-induced ionospheric electric fields at tropical latitudes. J Geophys Res Space Phys 102(A6):11521–11532. https://doi.org/10.1002/2014JD021594
Molinari J, Moore PK, Idone VP, Henderson RW, Saljoughy AB (1994) Cloud-to-ground lightning in Hurricane Andrew. J Geophys Res 99(D8):16665–16676. https://doi.org/10.1029/94JD00722
Molinari J, Moore P, Idone V (1999) Convective structure of hurricanes as revealed by lightning locations. Mon Weather Rev 127(4):520–534. https://doi.org/10.1175/1520-0493(1999)127%3c0520:Csohar%3e2.0.Co;2
Mondal SK, Chakrabarti SK, Sasmal S (2012) Detection of ionospheric perturbation due to a soft gamma ray repeater SGR J1550–5418 by very low frequency radio waves. Astrophys and Space Sci 341(2):259–264. https://doi.org/10.1007/s10509-012-1131-5
NaitAmor S, Ghalila H, Cohen M (2017) TLEs and early VLF events: simulating the important impact of transmitter-disturbance-receiver geometry. J Geophys Res: Space Physics 122(1):792–801. https://doi.org/10.1002/2016JA022791
NaitAmor S, Cohen M, Kumar S, Chanrion O, Neubert T (2018) VLF signal anomalies during cyclone activity in the Atlantic Ocean. J Geophys Res 45:10185–110192. https://doi.org/10.1029/2018GL078988
Nina A, Čadež V (2013) Detection of acoustic-gravity waves in lower ionosphere by VLF radio waves. Geophys Res Lett 40(18):4803–4807. https://doi.org/10.1002/grl.50931
Nina A, Simić S, Srećković VA, Popović LČ (2015) Detection of short-term response of the low ionosphere on gamma ray bursts. Geophys Res Letts 42(19):8250–8261. https://doi.org/10.1002/2015GL065726
Nina A, Radovanović M, Milovanović M, Kovačević A, Bajčetić J, Popović LČ (2017) Low ionospheric reactions on tropical depressions prior hurricanes. Adv in Space Res 60(8):1866–1877. https://doi.org/10.1016/j.asr.2017.05.024
Pal S, Hobara Y (2016) Mid-latitude atmosphere and ionosphere connection as revealed by very low frequency signals. J Atmos Sol-Terr Phys 138:227–232. https://doi.org/10.1016/j.jastp.2015.12.008
Pal S, Sarkar S, Midya SK, Mondal SK, Hobara Y (2020) Low-Latitude VLF radio signal disturbances due to the extremely severe cyclone Fani of May 2019 and associated mesospheric response. J Geophys Res Space Phys 125(5):e2019JA027288. https://doi.org/10.1029/2019JA027288
Poulsen WL, Inan US, Bell TF (1993) A multiple-mode three-dimensional model of VLF propagation in the Earth-ionosphere waveguide in the presence of localized D region disturbances. J Geophys Res 98(A2):1705–1717. https://doi.org/10.1029/92ja01529
Price C, Yair Y, Asfur M (2007) East African lightning as a precursor of Atlantic hurricane activity. Geophys Res Letts 34(9):L09805. https://doi.org/10.1029/2006GL028884
Qian L, Wang W, Burns AG, Chamberlin PC, Coster A, Zhang S-R, Solomon SC (2019) Solar Flare and geomagnetic storm effects on the thermosphere and ionosphere during 6–11 September 2017. J Geophys Res Space Phys 124(3):2298–2311. https://doi.org/10.1029/2018JA026175
Rodger CJ (2003) Subionospheric VLF perturbations associated with lightning discharges. J Atmosc Sol-Terr Phys 65(5):591–606. https://doi.org/10.1016/S1364-6826(02)00325-5
Rodger CJ, Brundell JB, Holzworth RH, Lay EH (2009) Growing detection efficiency of the world wide lightning location network, paper presented at AIP Conference Proceedings. https://doi.org/10.1063/1.3137706.
Rozhnoi A, Solovieva M, Levin B, Hayakawa M, Fedun V (2014) Meteorological effects in the lower ionosphere as based on VLF/LF signal observations. Nat Hazards Earth Syst Sci 14(10):2671–2679. https://doi.org/10.5194/nhess-14-2671-2014
Selvakumaran R, Maurya AK, Gokani SA, Veenadhari B, Kumar S, Venkatesham K, Phanikumar D, Singh AK, Siingh D, Singh R (2015) Solar flares induced D-region ionospheric and geomagnetic perturbations. J Atmos and Sol-Terr Phys 123:102–112. https://doi.org/10.1016/j.jastp.2014.12.009
Solorzano NN, Thomas J, Holzworth R (2008) Global studies of tropical cyclones using the World Wide Lightning Location Network, paper presented at the 3rd conference on meteorological applications of lightning data, 20–25 January 2008.
Thomas JN, Solorzano NN, Cummer SA, Holzworth RH (2010) Polarity and energetics of inner core lightning in three intense North Atlantic hurricanes. J Geophys Res Space Phys 115(A3):A00E15.https://doi.org/10.1029/2009JA014777.
Thomson NR, Rodger CJ, Clilverd MA (2005) Large solar flares and their ionospheric D region enhancements. J Geophys Res Space Phys 110(A6):A06306. https://doi.org/10.1029/2005ja011008
Thomson NR, Clilverd MA, McRae WM (2007) Nighttime ionospheric D region parameters from VLF phase and amplitude. J Geophys Res: Space Physics 112(A7):A07304. https://doi.org/10.1029/2007JA012271
Thomson NR, Rodger CJ, Clilverd MA (2011) Daytime D region parameters from long-path VLF phase and amplitude. J Geophys Res 116(A11):A11305. https://doi.org/10.1029/2011ja016910
Vadas SL, Taylor MJ, Pautet P-D, Stamus PA, Fritts DC, Liu H-L, Sabbas FTS, Rampinelli VT, Batista P, Takahashi H (2009) Convection: the likely source of the medium-scale gravity waves observed in the OH airglow layer near Brasilia, Brazil, during the SpreadFEx campaign. Ann Geophys 27(1):231–259. https://doi.org/10.5194/angeo-27-231
Venkatesham K, Singh R, Maurya AK, Dube A, Kumar S, Phanikumar D (2019) The 22 July 2009 total solar eclipse: modeling D region ionosphere using narrowband VLF observations. J Geophys Res Space Phys 124(1):616–627. https://doi.org/10.1029/2018JA026130
Wait JR (1962) Electromagnetic waves in stratified media. Pergamon Press, Oxford
Wait JR, Spies KP (1964) Characteristics of the earth-ionosphere waveguide for VLF radio waves. Technical Note 300, National Bureau of Standards, Boulder, Colorado
Xiao Z, Xiao SG, Hao YQ, Zhang DH (2007) Morphological features of ionospheric response to typhoon. J Geophys Res Space Phys 112(A4):A04304. https://doi.org/10.1029/2006JA011671
Xu W, Rutledge SA, Zhang W (2017) Relationships between total lightning, deep convection, and tropical cyclone intensity change. J Geophys Res 122(13):7047–7063. https://doi.org/10.1002/2017jd027072
Yigit E, Aylward AD, Medvedev AS (2008) Parameterization of the effects of vertically propagating gravity waves for thermosphere general circulation models: sensitivity study. J Geophys Res 113:D19106. https://doi.org/10.1029/2008JD010135
Zhang W, Zhang Y, Zheng D, Zhou X (2012) Lightning distribution and eyewall outbreaks in tropical cyclones during landfall. Mon Weather Rev 140:3573–3586. https://doi.org/10.1175/MWR-D-11-00347.1

Publisher's Note